CHAOS COMMUNICATION USING SEMICONDUCTOR LASERS SUBJECT TO DIFFERENT KINDS OF OPTICAL FEEDBACK

V.Z. Tronciu

Technical University of Moldova, 168, Stefan cel Mare ave., MD-2005, Chisinau, Republic of Moldova
Weierstrass Institute for Applied Analysis and Stochastics, 39, Mohren str., 10117, Berlin, Germany
Institute of Applied Physics, Academy of Sciences of Moldova, 5, Academiei str., MD-2028, Chisinau, Republic of Moldova
E-mail: tronciu@mail.utm.md
(Received 11 July 2009)

Abstract

In this review, we report the results of numerical investigations of the dynamical behavior of an integrated device composed by a semiconductor laser and different cavities that provide optical feedback. Due to the influence of the feedback, under the appropriate conditions the systems display chaotic behavior appropriate for chaos based communications. The optimal conditions for chaos generation are identified. It is found that the longitudinal double cavity feedback requires lower feedback strengths for developing high complexity chaos as compared with a single cavity. The synchronization of two unidirectional coupled (master-slave) systems and the influence of parameters mismatch on the synchronization quality are also studied. Examples of message encoding and decoding within chaos modulation technique for longitudinal double cavity optical feedback are presented and discussed. We find that the resynchronization time for the T-like double cavity optical feedback scheme can be two orders of magnitude shorter as compared with that of the single-cavity feedback case. Very good conditions for message encoding by using the on/off phase shift keying encryption method are identified, and examples of message encoding/decoding are presented.

1. Introduction

The synchronization of chaotic oscillators has been a subject of deep studies in the last years due to its fundamental and applied properties [1]. In terms of application, chaos based communications have become an option to improve privacy and security in data transmission, especially after the recent field demonstration on the metropolitan fiber networks of Athens [2]. In optical chaos based communications, the chaotic waveform is generated by using semiconductor lasers with either all-optical [3-7] or electro-optical [8-10] feedback loops. In particular, semiconductor lasers subject to the influence of optical feedback from a distant mirror have been investigated extensively for the past two decades, and different dynamical behaviors have been characterized, including periodic and quasi-periodic pulsations, low frequency fluctuations, and coherent collapse (for more detail, see Ref. [11]). In the Conventional all-Optical Feedback case (COF) typically, to achieve chaotic behavior a delay round trip time of at least a few hundreds of ps is needed. So, in the air, the external cavity should be about a few cm long, which is a drawback for the design of compact chaotic sources. Integrated lasers with ultra-short feedback cavities have also revealed similar characteristics if the

feedback is properly amplified [12]. In this context, multi-section lasers with an amplified feedback section could be suitable candidates for integrated chaotic emitters. Due to the continuing technological progress, multi-section lasers have stable and compact configurations, which include integrated sections with common waveguides and a tunable phase shift [13]. However, the simplest configuration, a two-section laser with one active section and one passive section acting as an external cavity, is not suitable since the length of the passive section is typically too short to achieve chaotic dynamics.

Lasers subject to feedback from two cavities have been considered in several configurations [14-18]. In particular, feedback from a second cavity has been used to control the chaotic dynamics of semiconductor lasers with optical feedback. Control in the low frequency fluctuation regime has been achieved by adjusting properly both the length and the feedback strength of the second external cavity. Configurations using Fabry-Perot resonators to provide feedback have also been studied [19, 20]. In this case, the feedback can destabilize the laser emission but can also improve the stability of continuous wave (CW) emission by enhancing the damping of relaxation oscillations or allowing the control of the chip in a non-invasive way.

Several ways for encoding and decoding a message within the chaotic carrier has been proposed in the literature, including chaos modulation [3], chaos shift keying [21], chaos masking [22], etc. Here we consider two kinds; the chaos modulation (CM) technique applied to longitudinal double cavity feedback scheme and On/Off Phase Shift Keying (OOPSK) method applied to T-like double cavity optical feedback setup (see Fig. 1). Finally, we mention that this review summarizes and completes the main results of [23] and [24].

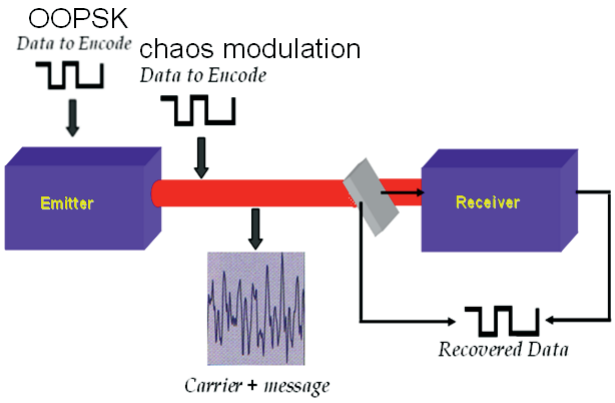

Fig. 1. Different schemes of message encryption.

The paper is structured as follows. In Section 2 we introduce an appropriate model to describe the dynamics of semiconductor laser under the influence of the longitudinal double cavity feedback (LDCF). We study the synchronization of two of such systems. The influence of the mismatch in the feedback phases on the synchronization quality is also discussed. Section 3 presents a study of the dynamics of a laser under the influence of a T-like double cavity optical feedback (TDCF). We highlight the advantages of the proposed setup when compared with the COF case and the OOPSK encryption method is demonstrated for the TDCF. The summary and conclusions are given in Section 4.

2. Longitudinal double cavity feedback. Chaos modulation technique

In this Section, we consider an integrated device composed of a semiconductor laser subject to feedback from a double cavity grown in longitudinal direction with the aim of generat-

ing a complex chaotic waveform suitable for applications in chaos based communications. The scheme of the system is depicted in Fig. 2. It consists of a single mode semiconductor laser coupled to an external passive cavity of the same III-V material through an air gap. Here we choose two external cavities (air gap and III-V material) of the same length, in this case 1 cm. To avoid diffraction losses in the air cavity, a micro lens should be placed at the laser facet to collimate the beam (not shown in our set-up). Assuming a refractive index of 3 for the material, the total delay time in the two cavities amounts approximately 0.266 ns. The advantage of this longitudinal double cavity configuration is the existence of two feedback phases, one in the air gap cavity and one in the material cavity, the latter can be easily adjusted to destabilize the dynamics of the laser. Moreover, while we assume that the first reflectivity is defined by the air-material facet, the outer facet of the material cavity can be coated to increase its reflectivity. We study the conditions for which the behavior of the system is chaotic due to the influence on the laser dynamics of the feedback from the double cavity. We also study the synchronization of two such systems under unidirectional coupling. In the absence of coupling, the behavior of transmitter and receiver systems is uncorrelated. When a certain amount of light is injected from the transmitter into the receiver, the latter is able to synchronize to the emitter under the appropriate conditions. Typically, the receiver does not synchronize identically to the emitter due to the injected field. Therefore, synchronization is not complete but generalized [25]. Synchronization is robust to small perturbations of the carrier. A message of small amplitude can then be included in the carrier which will be filtered-out by the receiver. As mentioned above, several message-encoding schemes have been proposed in the literature. Here we include the message as a modulation in the amplitude of the chaotic carrier (chaos modulation) [3] (see Fig. 1). The message can be decoded at the receiver by comparing its input (carrier mixed with message) with its output (which ideally reproduces only the carrier).

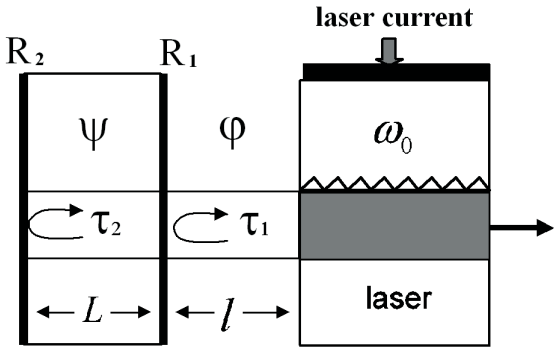

Fig. 2. A sketch of the proposed setup for chaos synchronization and message encoding, using semiconductor lasers under the influence of a feedback from a double cavity grown in longitudinal direction. R_1 and R_2 are the reflectivity of the air-material facet and the outer facet of the material cavity, respectively. The length of the air cavity l and the material cavity L are taken to be the same: $L = l = 1$ cm, $n_L = 3$; ω_0 is the free running frequency of CW laser.

2.1. Model and equations

To model the set-up shown in Fig. 2 we consider a single mode CW laser coupled to a longitudinal double cavity. The first mirror is located at distance l from the laser facet. The distance between the first and second mirror is L. The optical feedback phase in the second cavity ψ can be controlled by injecting current into the passive section. We assume that the current injected in

the passive section is small enough to affect only the refractive index, so that the optical length of the resonator is changed in the sub-wavelength range. In this way, while the feedback phase ψ can be tuned, the change in the delay time between the two mirrors τ_L is negligible. Alternatively, this phase could be also controlled with a piezo actuator. In principle, multiple reflections may take place. However, for the feedback parameters we will use, it is sufficient to consider a single reflection in both cavities. This approximation strongly simplifies the calculations.

The laser dynamics can be analyzed in the framework of the extended Lang-Kobayashi equations for the complex field amplitude E and an excess carrier density N [26, 27]

$$\begin{aligned}\frac{dE_{t,r}}{dt} &= (1+i\alpha)\left[\frac{g(N_{t,r}-N_0)}{1+\varepsilon\left|E_{t,r}\right|^2}-\frac{1}{\tau_{ph}}\right]\frac{E_{t,r}}{2}+F_{LDCF}+k_rE_t \\ \frac{dN_{t,r}}{dt} &= \frac{I_{t,r}}{e}-\frac{1}{\tau_e}N_{t,r}-\frac{g(N_{t,r}-N_0)}{1+\varepsilon\left|E_{t,r}\right|^2}\left|E_{t,r}\right|^2\end{aligned} \tag{1}$$

where the feedback term is written as

$$F_{LDCF}=\gamma_{t1,r1}e^{-i\varphi}E_{t,r}(t-\tau_l)+\gamma_{t2,r2}e^{-i(\varphi+\psi)}E_{t,r}(t-(\tau_l+\tau_L)). \tag{2}$$

The subscripts t and r refer to transmitter and receiver lasers, respectively. The last term in equation (1) is present only in the receiver laser and describes the unidirectional coupling; k_r is the coupling parameter of the injected field into the receiver laser given by $\kappa_r=\sqrt{1-R}\eta_{ext}\Big/\left(\tau_c\sqrt{R}\right)$, where R is the facet power reflectivity of the slave laser (R = 30%), τ_c is the cavity roundtrip time of the light within the laser ($\tau_c=10$ ps), η_{ext} accounts for losses different than those introduced by the laser facet ($\eta_{ext}=0.5$); τ_l and τ_L are the air gap and passive material roundtrip times, respectively; $\gamma_{t1,r1}$ and $\gamma_{t2,r2}$ are the feedback strengths governed by the reflectivity R_1 and R_2, respectively. For simplicity, we assume R_1 and R_2 such that $\gamma_{t1}=\gamma_{t2}=\gamma_{r1}=\gamma_{r2}=\gamma$; $\varphi=\omega_0\tau_l$ (whose value can strongly vary in different devices), and $\psi=\omega_0\tau_L$ are the optical phase accumulated in the air gap and material cavities, respectively. The other parameter values are the linewidth enhancement factor α = 5, the differential gain parameter $g=1.5\times10^{-8}$ ps^{-1}, the gain saturation coefficient $\varepsilon=5\times10^{-7}$, the photon and carrier lifetimes τ_{ph} = 3 ps and τ_e = 2 ns, respectively, and the round trip times τ_l = 0.066 ns and τ_L = 0.2 ns. The injected current is fixed at $I=50$ mA (the threshold current I_{th} = 11.5 mA) and the currier number at the transparency at $N_0=1.2\times10^8$. The parameter values are used for the calculated results that are shown in all figures of the paper.

2.2. Stationary states

In the subsequent analysis, we consider the stationary lasing states of system (1)-(2). They are given by rotating wave solutions, usually called External Cavity Modes (ECMs)

$$E(t)=E_Se^{i\omega_St},\ N=N_S. \tag{3}$$

By substituting (3) into (1)-(2), we obtain the transcendental equation for the emission frequency ω_S

$$\begin{aligned}F(\omega_S) = &-\omega_S+\alpha\gamma\left[-\cos(\varphi+\omega_S\tau_l)-\cos(\varphi+\psi+\omega_S(\tau_l+\tau_L)\right]- \\ &-\gamma\left[\sin(\varphi+\omega_S\tau_l)+\sin(\varphi+\psi+\omega_S(\tau_l+\tau_L))\right],\end{aligned} \tag{4}$$

ω_S is obtained from $F(\omega_S) = 0$. Finally, E_s and N_s can be obtained by substituting the value of ω_S into (1) and (2) and by setting roots to zero.

When only one cavity is present (COF), eq. (4) provides a finite number of solutions which are located on top of an ellipse in the N_S vs. ω_S plane. This elliptical locus for the solutions is independent of the feedback phase $\omega_S\tau$, being τ the external cavity round trip time. The feedback phase then determines the exact number of solutions as well as its precise location on the ellipse. If the feedback phase is changed, the location of the solutions moves around the ellipse.

In contrast to the COF case, the feedback from Fabry-Perot resonator implies a non elliptic location of modes [19]. For different phases φ, the location of the ECMs moves along an eight-shape figure, with the solitary laser mode located in the waist. The nature of the bifurcations and the stability of the solutions for the resonant feedback from FPR have been analyzed in more detail in [19].

The situation is again different for the case of LDCF. The solid lines in Fig. 3 show the locus of ECMs in the plane ($N_S - \omega_S$) for two different levels of feedback strength and three different values of one of the feedback phases, φ. The other feedback phase, ψ, determines then the exact number of solutions and its precise location of the solutions on the geometrical locus shown in Fig. 3. We first consider small feedback strength $\gamma = 5\ \mathrm{ns}^{-1}$ (left column in Fig. 3). For $\varphi = -\pi/2$, the location of the fixed points is similar to that of COF case, i.e., the modes are located on the ellipse although now the ellipse is distorted (see Fig. 3a left). Different symbols show the precise location of ECMs at particular feedback phases ψ. Note that the number of ECM depends on the values of the feedback phase. For $\psi = -\pi$ two modes and one anti-mode coexist (circles). On the other hand, only one mode is present for $\psi = 0$ (triangle) and $\psi = \pi/4$ (square). For $\varphi = \pi/6$ the system exhibits almost the tilted eight-shape (see Fig. 3b left) which is similar to that found in a Fabry–Perot resonator [18]. Although the level of feedback is still the same as before, the number of solutions has increased for all the values of the feedback phase ψ. Note also that the size of the locus for the ECMs is clearly larger than in the previous case. Finally, for $\varphi = \pi/2$ the tilted eight shape opens in the center leading to a "peanut" shape for the locus of the ECMs (see Fig. 3c left). The overall size of the locus, as well as the approximate number of solutions, is the same as for $\varphi = \pi/6$. This clearly illustrates that, in the case of the LDCF, the location of the modes becomes more complicated as compared with that of COF. When the feedback strength is increased to $\gamma = 15\ \mathrm{ns}^{-1}$ (right column in Fig. 3) new satellite bubbles of ECMs appear on left and right sides of the deformed ellipse. The different satellite bubbles span for a range of frequencies which is much larger than for the weak feedback case $\gamma = 5\ \mathrm{ns}^{-1}$. The onset of these bubbles reflects the existence of frequency gaps for which no ECM solutions exist. These frequency gaps are originated from destructive interference in the feedback coming from the two cavities. Figure 4a shows the total reflected light for the parameters corresponding to the right panel of Fig. 3a. Within the range of frequencies in which ECM solutions are found, there are two regions of vanishing reflected light which correspond to the two regions that separate the three bubbles shown in the right panel of Fig. 3a.

The interference of the feedback from the two cavities leads to an effective vanishing feedback, so there are no external cavity modes. Figure 4b shows the value of the roots of Eq. (4) for the parameters of the left panel of Fig. 3a and $\varphi = -\pi/2$. It can be seen as a fast oscillatory behavior on the top of a slower one. The fast and slow oscillatory periods are determined by the two feedback times. The intersection of this curve with the diagonal signals the

solutions of Eq. (4). As γ increases, the amplitude of the oscillations becomes larger and therefore more ECMs exist for any given value of the feedback phases. The feedback strength increase leads also to the emergence of additional isles of ECMs. The precise location of the bubbles and their shape depend on the feedback phase as shown in the right column of Fig. 3.

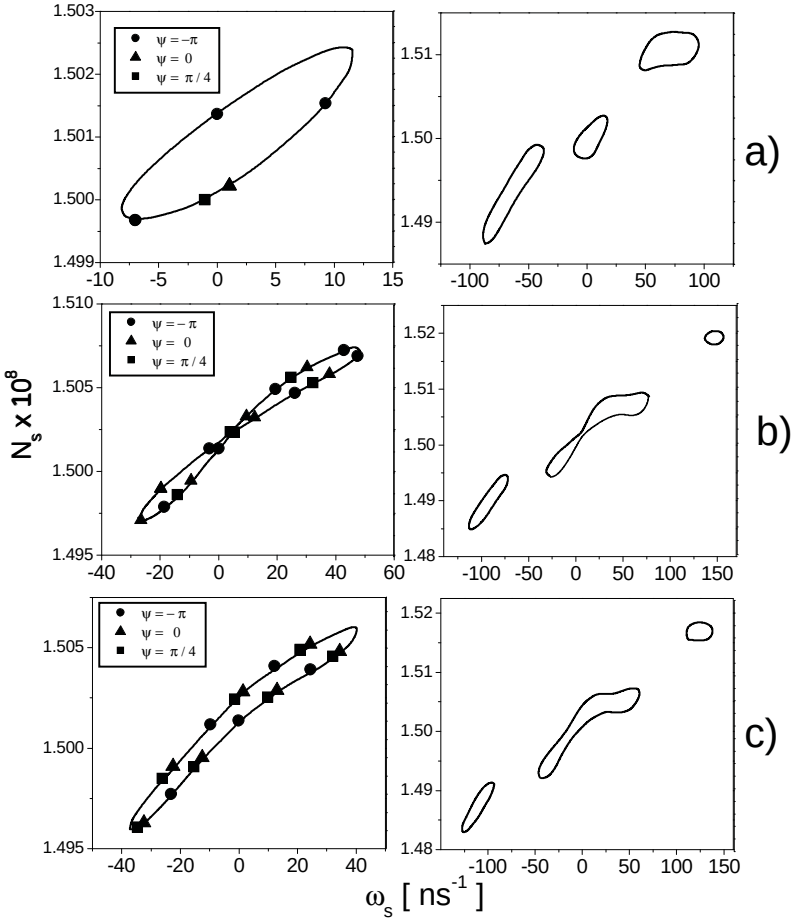

Fig. 3. Locus of the ECMs in the plane ($N_S - \omega_S$) for different phases: (a) $\varphi = -\pi/2$, (b) $\varphi = \pi/6$, and (c) $\varphi = \pi/2$ and two levels of feedback strength: $\gamma = 5\ \mathrm{ns}^{-1}$ (left) and $\gamma = 15\ \mathrm{ns}^{-1}$ (right). Symbols indicate the external cavity modes for a specific value of the feedback phase ψ.

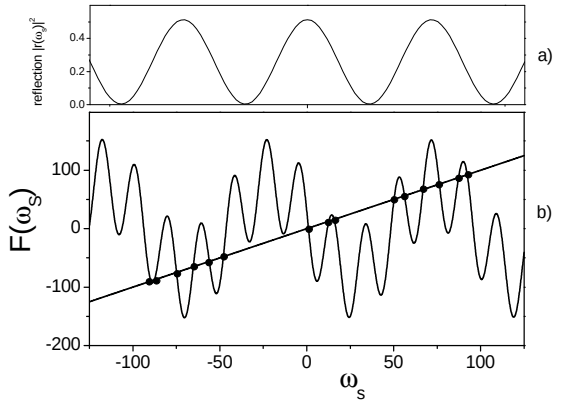

Fig. 4. Reflection spectrum of a double cavity with $\gamma = 15\ \mathrm{ns}^{-1}$ (a) and graphical solution of (4) (b) for $\gamma = 15\ \mathrm{ns}^{-1}$, $\varphi = -\pi/2$, and $\psi = \pi/4$. The circles indicate the modes.

2.3. Chaotic behavior of the LDCF transmitter laser

For feedback strength small enough, a laser under the influence of COF or LDCF shows either CW or pulsating operation. Chaotic behavior appears as the feedback strength is increased. Figure 5 illustrates typical time traces (left) and the power spectra (right) of a semiconductor laser under the influence of COF and LDCF for identical laser parameters in the chaotic regime. It can be observed that the LDCF makes the laser behavior more complex. This fact was further confirmed by calculation of the autocorrelation time from Eqs. (3) $T_c = \int_0^\infty d\tau\ \Gamma_{ii}^2(\tau)$ and (4) $\Gamma_{ij}(\tau) = \left\langle \left(P_i(t) - \langle P_i \rangle\right)\left(P_j(t-\tau) - \langle P_j \rangle\right)\right\rangle \Big/ \sqrt{\left\langle \left(P_i(t) - \langle P_i \rangle\right)^2 \right\rangle \left\langle \left(P_j(t) - \langle P_j \rangle\right)^2 \right\rangle}$ of [12]. These calculations yield to $T_c^{COF} \approx 0.1$ ns and $T_c^{DCF} \approx 0.037$ ns. Moreover, larger amplitude fluctuations when compared with COF can be observed.

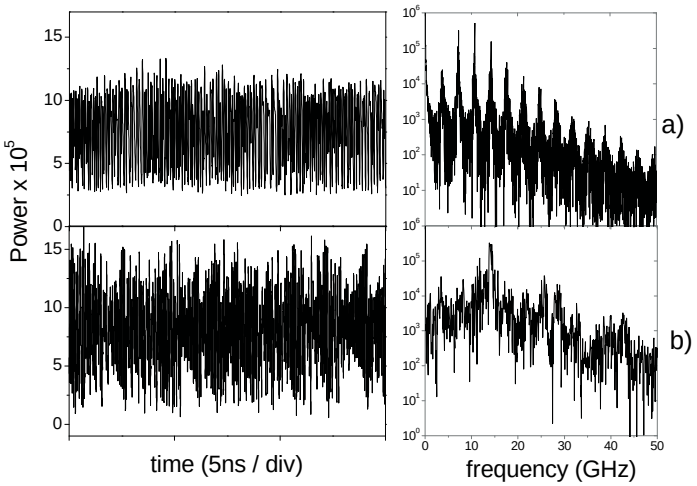

Fig. 5. A typical optical power time trace (left) and the power spectrum (right) of a semiconductor laser under the influence of (a) COF for $\gamma = 30\ \text{ns}^{-1}$, $\varphi = -\pi/2$, $\tau = 0.266$ ns and (b) DCF for $\gamma_1 = \gamma_2 = 30\ \text{ns}^{-1}$, $\varphi = -\pi/2$, $\psi = \pi$, $\tau = \tau_l + \tau_L = 0.266$ ns, $\tau_l = 0.066$ ns, $\tau_L = 0.2$ ns.

Figure 6 displays the bifurcation diagrams of the semiconductor laser subject to LDCF for two feedback phases. As the feedback strength is increased, several instabilities take place. For a given value of the feedback strength, the figure displays the values of all the local maxima of the time traces of the emitted power. Considering $\varphi = -\pi/2$ and $\psi = \pi$, for low values of the feedback strength, CW operation is observed, which is depicted as a single value for the maxima of the power in Fig. 6a. At the feedback strength $\gamma = 10\ \text{ns}^{-1}$ a Hopf bifurcation appears and the output power develops an oscillatory behavior. Since the oscillations are periodic, for a given feedback strength, all the local maxima of the output power have the same value and consequently a single point appears in Fig. 6. The Hopf bifurcation is supercritical and, as expected, the oscillation amplitude grows with the square root of the distance from the bifurcation point. As the feedback strength is further increased, a scenario compatible with quasi-periodic route to chaos is obtained. However, the range and amplitude of this behavior are small. When the feedback strength reaches the value $\gamma = 15\ \text{ns}^{-1}$, a jump to a new *P* periodic operation region is observed. As the feedback strength increases, a second scenario compatible with quasi-periodic route to chaos appears. For large values of the feedback strength, the system exhibits a chaotic behavior.

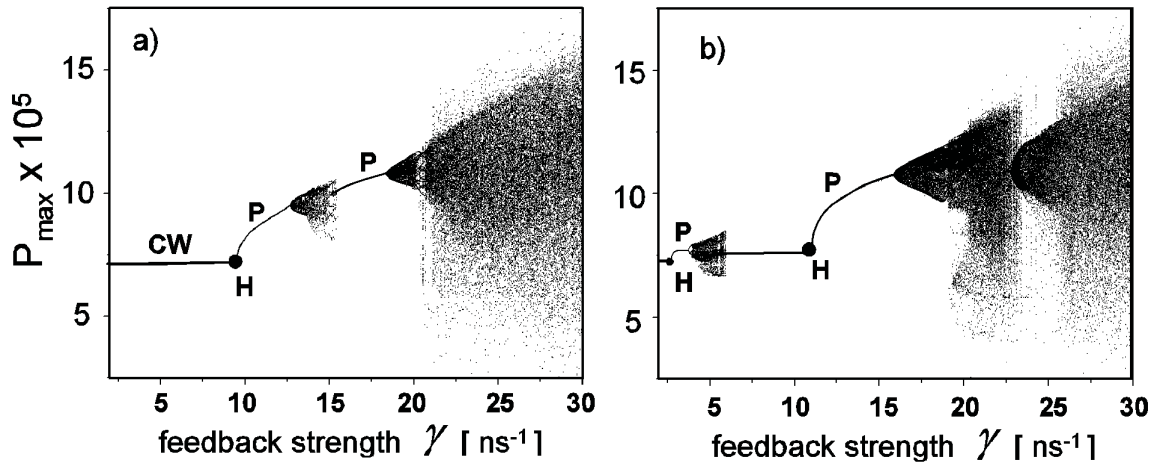

Fig. 6. Numerical bifurcation diagrams for different values of phases: (a) $\varphi = -\pi/2,\ \psi = \pi$ and (b) $\varphi = \pi/2,\ \psi = \pi/4$. CW shows the continuous-wave operation, the circle H indicates Hopf bifurcation, and P shows the peak of stable periodic solution.

For $\varphi = \pi/2$ and $\psi = \pi/4$ (see Fig. 6b) the system behavior is slightly different; the Hopf bifurcation is shifted to a lower feedback level involving the appearance of low amplitude chaotic behavior for low feedback strengths followed by the CW operation and a scenario compatible with quasi-periodic route to chaos. We mention that the numerical calculations show that, in this parameter region and for any value of the feedback strength larger than $25\ \text{ns}^{-1}$ and combination of phases φ and ψ, the laser behavior is chaotic and robust.

2.4. Synchronization and mismatch in the laser parameters

In the previous section, we have clarified different aspects of the dynamics of a semiconductor laser with integrated DCF for obtaining chaotic behaviors. In what follows, we are interested in the transmitter–receiver configuration and in the evaluation of their synchronization properties. Synchronization can be quantified by measuring the cross correlation coefficient:

$$\left[C = \langle P_m(t)P_s(t)\rangle / \left(\langle |P_m(t)|\rangle \langle |P_m(t)|\rangle\right)\right]. \tag{5}$$

Figure 7 shows the emitted power of slave system versus the power of the master (synchronization diagram) for feedback strength $\gamma = 30\ \text{ns}^{-1}$ and different levels of the coupling parameter k. We first consider the case of identical Master and Slave systems, so we take the same parameter values for both of them. When the coupling parameter is equal to zero, as shown in Fig. 7a, the trajectories of the master and slave lasers depart from each other and the synchronization map is a cloud of points showing the lack of correlation between outputs. Upon increasing the coupling until $100\ \text{ns}^{-1}$, the synchronization improves and cross correlation coefficient increases approaching one (see Fig. 7c).

Figure 8 shows the dependence of the synchronization quality as a function of the feedback phases. It displays the value of the correlation function in the parameter space $(\varphi - \psi)$ for feedback strength $\gamma = 30\ \text{ns}^{-1}$ and coupling coefficient $\kappa = 75\ \text{ns}^{-1}$. It can be clearly seen that the region of high correlation coefficients is wide while regions of low correlation hardly appear. The white star in Fig. 8 corresponds to the operating point that will be considered for message encoding and decoding in the next section.

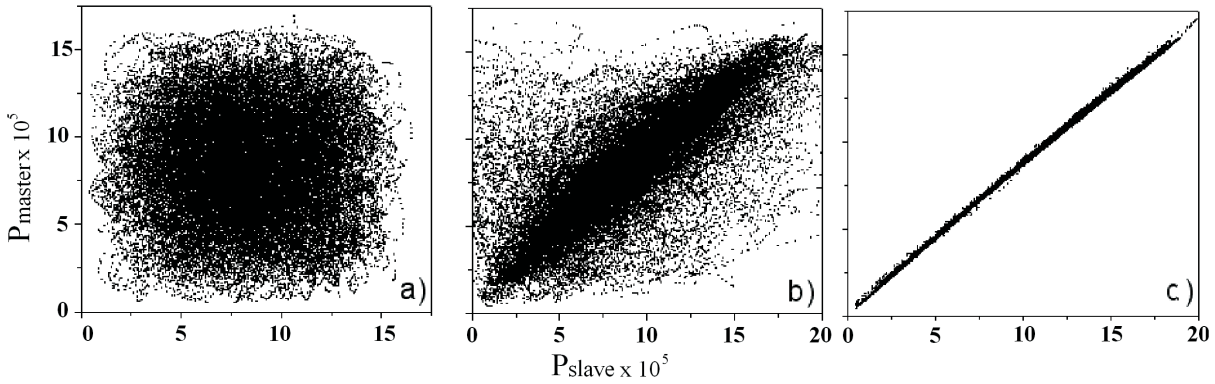

Fig. 7. Synchronization diagrams for different levels of the coupling parameter k: (a) $k = 0\ \mathrm{ns}^{-1}$ (the systems are uncorrelated), (b) $k = 50\ \mathrm{ns}^{-1}$ (C=0.75), and (c) $k = 100\ \mathrm{ns}^{-1}$ (C=0.9995). The feedback strength is taken as $\gamma = 30\ \mathrm{ns}^{-1}$ and the feedback phases are $\varphi = -\pi/2$ and $\psi = \pi$.

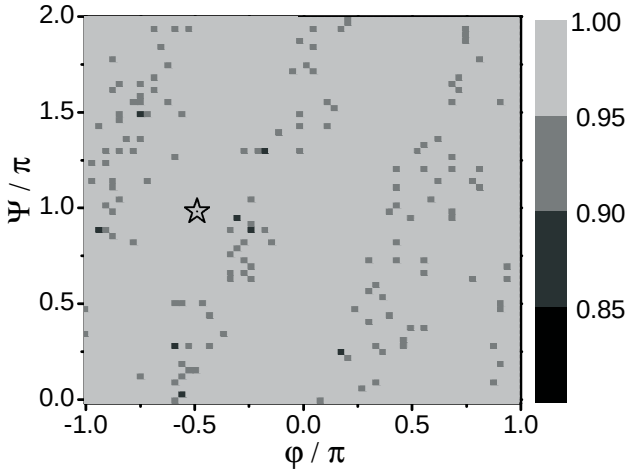

Fig. 8. Cross correlation coefficient as a function of the feedback phases for $\gamma = 30\ \mathrm{ns}^{-1}$ and $\kappa = 75\ \mathrm{ns}^{-1}$. The white star is the operating point for the message encoding and decoding.

It is well known that the quality of the synchronization depends on the similarity between master and slave lasers. The influence of the internal laser parameters mismatch on the synchronization quality has been studied in [22, 28], so here we focus on the influence of the mismatch on the two feedback phases. Figure 9 shows the dependence of cross correlation coefficient on the phase difference (phase master–phase slave) for feedback strength $\gamma = 30\ \mathrm{ns}^{-1}$ and coupling strength $k = 75\ \mathrm{ns}^{-1}$ (a) and $k = 100\ \mathrm{ns}^{-1}$ (b). The solid line shows the degradation of the synchronization due to a mismatch in the material cavity feedback phase. We take $\varphi_m = \varphi_S = \pi$ and $\psi_s = 0$ while ψ_m is varied from 0 to π. The dotted line shows the effect of a mismatch in the air cavity feedback phase. We consider $\psi_s = \psi_m = \pi$ and $\varphi_S = 0$ while φ_m is varied from 0 to π. When the feedback phases coincide, the system exhibits perfect synchronization with C ~ 1 cross-correlation coefficient. An increase of the mismatch in any of the feedback phases induces a degradation of the synchronization which is indicated by a reduction of the cross correlation coefficient. For small mismatch, the degradation of the correlation is similar for the mismatch in any of the two phases.

As the mismatch is increased, the degradation is clearly more severe in the case of mismatch in the feedback phase of the air cavity φ.

This may be understood from the fact that φ is the phase of a shorter cavity and, in general, short cavities are more sensitive to phase variations than long cavities. For larger values of the coupling strength, the effect of the mismatch in the feedback phases is smaller and therefore the cross-correlation coefficient decreases slower as the mismatch is increased. High values of the cross-correlation coefficient are usually required for efficient message encoding and decoding, therefore, the mismatch in the feedback phases should not exceed $0.1/\pi$. Alternatively, a small airgap phase mismatch can be compensated adjusting the material phase ψ of the slave laser. Figure 9c shows an example of this compensation. The mismatch in the airgap phase is 2.5% (point *B* in Fig. 9a), and a very good correlation can be achieved (point *C*).

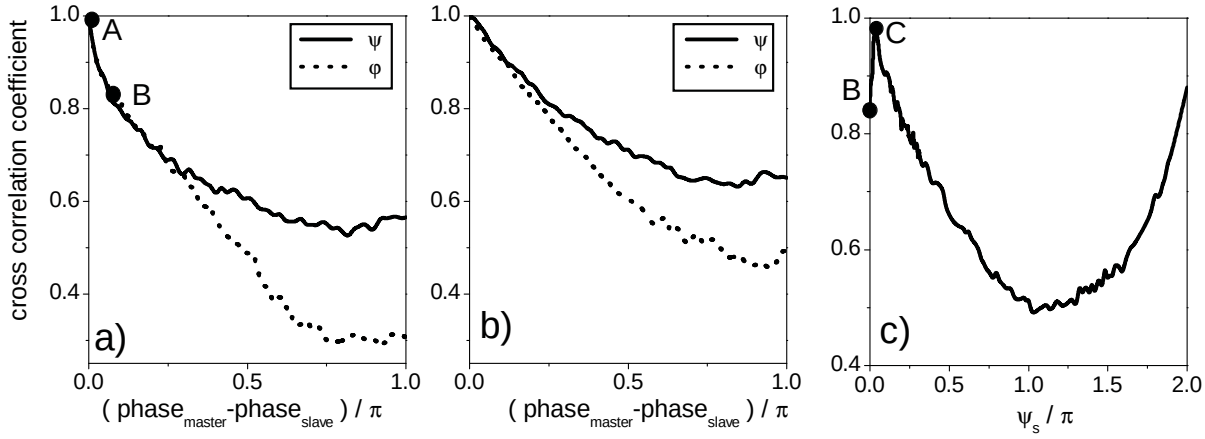

Fig. 9. Cross correlation coefficient as a function of the feedback phase difference (phase master–phase slave) for coupling $k = 75\ \text{ns}^{-1}$ (a), to $k = 100\ \text{ns}^{-1}$ (b). Panel (c) shows the cross correlation coefficient for $\varphi_m = \varphi_S = \pi$, and $\psi_m = 0$ as a function of the material phase for the slave laser ψ_s. For both master and slave systems, the feedback strength was taken as $\gamma = 30\ \text{ns}^{-1}$ (from [23]).

2.5. Message transmission

In this section, we consider the use of these integrated devices for message encoding and decoding in chaos based communications. A message is encoded as a small amplitude modulation of the emitted field of the master, so that the signal transmitted to the receiver is

$$E_T = E_t(1+\varsigma m(t)), \tag{6}$$

where $m(t)$ is the message and ς is the message amplitude. In the receiver system, a message is decoded comparing the input of the receiver with its output, which is ideally synchronized to the carrier

$$M_{decoded} = \sqrt{P_T / P_S} - 1. \tag{7}$$

Figure 10 illustrates the transmission of a non return to zero pseudorandom message. The system parameters correspond to the operating point shown by the white star in Fig. 8. Panel (a) shows the input message. Panels (b) and (c) show the chaotic carrier without the message and the transmitted signal (carrier with message). Panel (d) shows the decoded message as indicated in Eq. (7), and filtered by an appropriate low-pass filter [29]. As can be seen from the figure, the message is well recovered. Panel (e) shows the recovered message for a 2.5% mis-

match in the airgap phases between master and slave lasers. It can be clearly seen that a part of message cannot be recovered. On the other hand the airgap phase mismatch can be compensated by the controllable phase of slave laser. As can be seen in panel (f), the message is now well recovered.

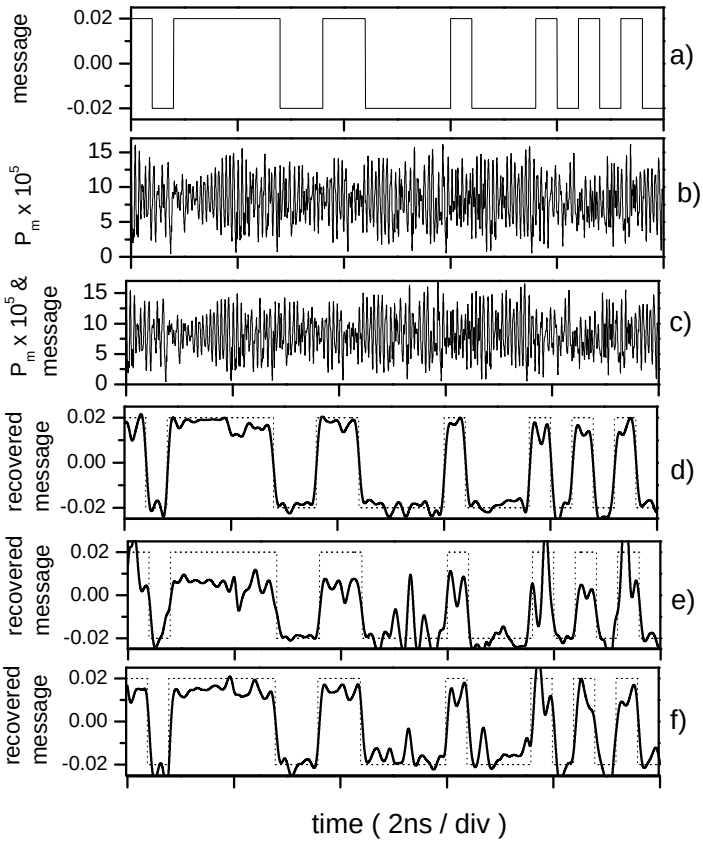

Fig. 10. Numerical results of encoding and decoding of a 2.5 Gbit/s digital message for a closed loop scheme [23]: (a) encoded message, (b) output of master laser, (c) output of master laser with message, (d) recovered message after filtering (solid line) and input message (dotted line) for identical parameters for master and slave lasers (point *A* in Fig. 9a), (e) recovered message (solid line) after filtering for lasers with 2.5% mismatch of airgap phases (point *B* in Fig. 9a), (f) recovered message (solid line) after filtering for lasers with 2.5% mismatch of airgap phases but the slave air gap phase is compensated by a different ψ_s phase (point *C* in Fig. 9c). Parameters $\gamma = 30\ \mathrm{ns}^{-1}$, $\kappa = 75\ \mathrm{ns}^{-1}$, $\varphi = -\pi/2$, $\psi = \pi$, $\tau_l = 0.066$ ns, $\tau_L = 0.2$ ns.

It is noteworthy that these simple examples of the chaos modulation encoding technique, within a chaotic waveform, obtained from a double cavity feedback are efficient and simple and could be easily applied to a chaos-based communication system by using an external modulation.

3. T-like double cavity optical feedback. On/off phase shift keying method

One of the most attractive schemes in terms of security is the OOPSK method [21, 30] where the codification is achieved by slight modulating the phase of the optical feedback of the emitter (see Fig. 1). The physical basis for OOPSK is that the synchronization behavior of the receiver acts as a sensitive detector for variations of the transmitter feedback phase: suitable discrete changes yield the dynamics of the receiver to jump between synchronized and desynchronized states. In contrast to these drastic changes in the receiver dynamics, changes in the emitter dynamics should be noticeable neither in the intensity dynamics nor in the RF nor optical spectra. The principle of the ON/OFF phase shift keying encryption is as follows. The message is encoded by switching between two states of the master system that yield highly correlated (synchronized) states (Bit "0") or less correlated (desynchronized) states (Bit "1") in the receiver system. Hence, the message can be simply recovered by monitoring the synchronization error. The controlled variations in the master system can be accomplished by inserting, e.g., an electrooptical modulator within the external cavity of the transmitter. The message is decoded by detecting whether the receiver synchronizes or not with the input carrier [26]. Up to now, this technique has the disadvantage that the maximum modulation rate is only a few tens of Mbit/s [21, 30, 31].

3.1. Laser and feedback model

The proposed setup for implementation of OOPSK method is depicted schematically in Fig. 11. It consists of a semiconductor laser coupled to the external reflectors R_1 and R_2, that could be implemented, e.g., by using two fiber cavities. The advantage of the proposed scheme is that we can control two feedback strengths, two feedback phases, and two delay times independently. The feedback branch governed by reflectivity R_1 is called conventional feedback branch (CFB); the one governed by R_2, the modulated feedback branch (MFB). Assuming fiber based cavities with a refractive index of 1.5, we consider the delay time in the CFB to be $\tau_l = 0.5$ ns and that of MFB $\tau_L = 0.3$ ns. In the model, we only account for single reflexions in both branches. In the absence of coupling, the correlation between the transmitter and receiver outputs is negligible. When a certain amount of light from the transmitter is injected into the receiver, the latter is able to synchronize to the emitter under appropriate conditions. Once synchronized, a message can be encoded into the carrier. At the receiver side, the message can be recovered via the chaos pass filtering process [29].

The laser dynamics is analyzed in the framework of the extended Lang-Kobayashi equations well explained in Section 2 with the following feedback term

$$F_{TDCF} = \gamma_1 e^{i\varphi} E_{t,r}(t-\tau_1) + \gamma_2 e^{i\psi} E_{t,r}(t-\tau_2). \tag{8}$$

The cavity roundtrip time of the light within the laser is ($\tau_c = 8.5$ ps), η_{ext} accounts for losses different than those introduced by the laser facet ($\eta_{ext} = 0.5$) resulting in $\kappa = 90\ \text{ns}^{-1}$; τ_1 and τ_2 are roundtrip time in the CFB and MFB, respectively; γ_1 and γ_2 are the feedback strengths governed by the reflectivities R_1 and R_2, respectively; $\varphi = \omega_0 \tau_l$ and $\psi = \omega_0 \tau_L$ are the accumulated optical phases in the CFB and MFB, respectively, which, without loss of generality, can be assumed to take values between 0 and 2π. The other parameter values are: the linewidth enhancement factor $\alpha = 5$, the differential gain parameter $g = 1.5\times10^{-5}\ \text{ns}^{-1}$, the gain saturation coefficient $s = 4\times10^{-7}$, the photon and carrier lifetimes $\tau_{ph} = 2$ ps and $\tau_e = 2.0$ ns, respectively, and the carrier number at the transparency $N_0=1.5x10^8$. These parameters, which are considered identical for both lasers, are used for the calculated results shown in all figures in the paper. The injection current is fixed at $I = 45$ mA (I_{th}=14.7 mA). For the model given by equations (8) and (9), if $\tau_1 = \tau_2$ the feedback term in (8) can be reduced to a COF term with an equivalent feedback coefficient given by $\tilde{\gamma} e^{i\tilde{\varphi}} = \gamma_1 e^{i\varphi} + \gamma_2 e^{i\psi}$.

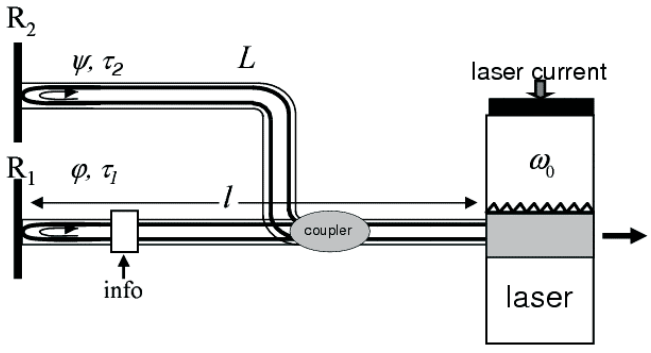

Fig. 11. Setup under study: a laser with fiber-based external cavities. The cavity lengths are l = 0.05 m (τ_1 = 0.5 ns) and L = 0.03 m (τ_2 = 0.3 ns). The refractive index of the optical fiber is n = 1.5.

3.2. TDCF transmitter laser dynamics

In this section, we discuss the behavior of a semiconductor laser under the influence of a TDCF. For feedback strengths small enough, semiconductor lasers under the influence of either COF or TDCF show CW or pulsating operations. Chaotic behavior appears if the feedback strength is increased enough. Figure 12b illustrates typical time traces (left) and the power spectra (right) of a laser under the influence of a DCF operating in a robust chaotic regime. We mention that the behavior shown in Fig. 12a is similar to that of a laser under the influence of COF with $\gamma_1 = 40\ \text{ns}^{-1}$, $\tau = 0.5\ \text{ns}$ and identical laser parameters. It is well known that the autocorrelation time is related to the complexity of the generated chaos. The correlation time accounts for the complexity of the generated chaos. The shorter is the correlation time, the more chaotic and less predictable is the dynamics. The calculations of the autocorrelation time for the traces shown in Figs. 12a and 12b [12] yield similar result for both COF and TDCF with values of $T_{ac}^{\ COF} \sim T_{ac}^{\ TDCF} \sim 100$ ps for our parameter values.

A confirmation of this property is given below. Figure 13a shows the autocorrelation time as a function of feedback strength for COF for $\tau = 0.5\ \text{ns}$ (solid line) and $\tau = 2\ \text{ns}$ (dotted line). It can be clearly seen that, as the feedback strength and delay time are increased, the autocorrelation time decreases; this is an indication that the laser dynamics becomes more chaotic. Figure 13b shows the calculated autocorrelation time for a laser under the influence of a TDCF. The feedback strength of CFB is fixed to $\gamma_1 = 30\ \text{ns}^{-1}$ while that of MFB is varied. For zero MFB strength, the resynchronization and autocorrelation times coincide with that of COF for $\gamma = 30\ \text{ns}^{-1}$. An increase in feedback strength of MFB leads to a decrease in autocorrelation time up to 0.1 ns similar to that of COF. However, when the MFB is introduced, the resynchronization time can be expected to become much shorter as a result of only distortion of the chaotic attractor generated by the CFB.

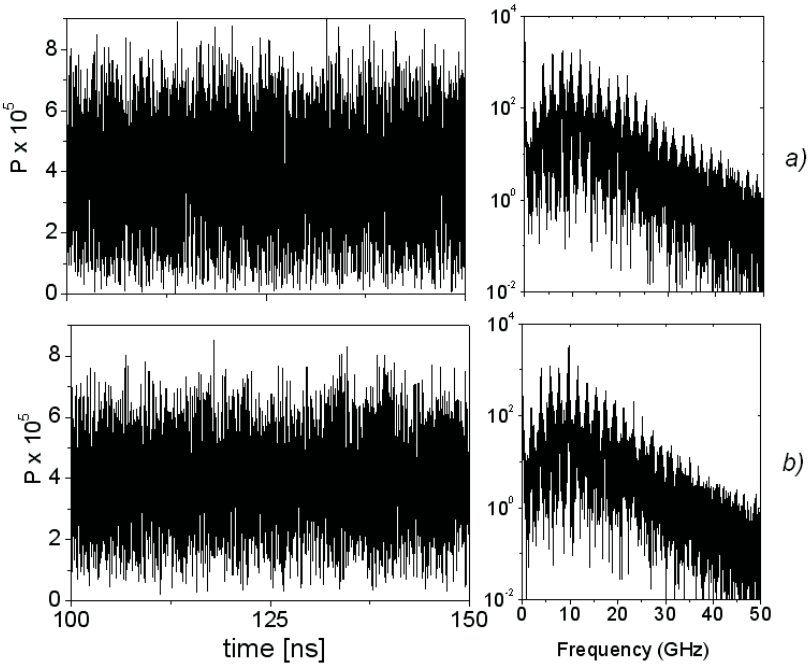

Fig. 12. Time traces of the output power P (left) and the power spectrum (right) for (a) COF at $\gamma = 40\ \text{ns}^{-1}$, $\tau = 0.5\ \text{ns}$, and $\varphi = 0$ and for (b) TDCF at $\gamma_1 = 30\ \text{ns}^{-1}$, $\gamma_2 = 10\ \text{ns}^{-1}$, $\tau_1 = 0.5\ \text{ns}$, $\tau_2 = 0.3\ \text{ns}$, $\varphi = 0$, and $\psi = \pi/2$.

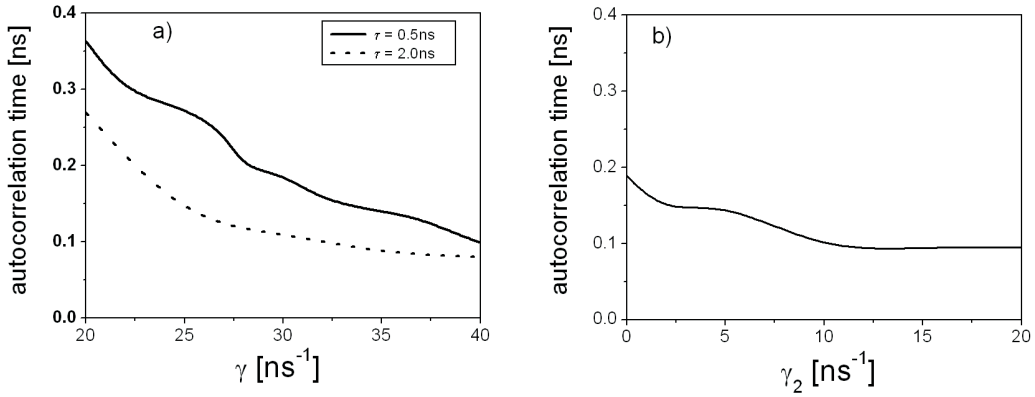

Fig. 13. The autocorrelation time as a function of feedback strength for (a) COF at $\varphi = 0$ and different values of delay time and (b) TDCF of MFB at $\gamma_1 = 30\ \text{ns}^{-1}$, $\varphi = 0$, $\psi = \pi/2$, $\tau_1 = 0.5$ ns, $\tau_2 = 0.3$ ns.

Figure 14a displays a typical bifurcation diagram of a semiconductor laser under the influence of COF with the feedback strength acting as a bifurcation parameter and $\tau = 0.5$ ns, $\varphi = 0$. As the feedback strength is increased, several bifurcations take place. For each value of the feedback strength, the figure displays the values of the maxima of the time traces of the emitted power. It is well known that, as the feedback strength is increased, a scenario compatible with quasi-periodic route to chaos appears [32].

Figures 14b and 14c display the bifurcation diagrams of a semiconductor laser subject to DCF for the feedback strength and feedback phase acting as bifurcation parameters. Let us consider, e.g., the case of feedback strength for the CFB fixed to $\gamma_1 = 30\ \text{ns}^{-1}$ while the feedback strength of MFB is increased. Considering $\varphi = 0$ and $\psi = \pi/2$, as shown in Fig. 14b, even for low values of the feedback strength γ_2 the dynamics of the laser is already chaotic due to the influence of the feedback of CFB. It can be noticed from the figure that the amplitude of the chaotic oscillations slightly increases with the feedback strength γ_2 (see Fig. 14b). When both feedback strengths are fixed to $\gamma_1 = 30\ \text{ns}^{-1}$, $\gamma_2 = 10\ \text{ns}^{-1}$ and the phase $\varphi = 0$, as shown in Fig. 14c, fully developed chaotic dynamics is found for any value of MFB phase ψ.

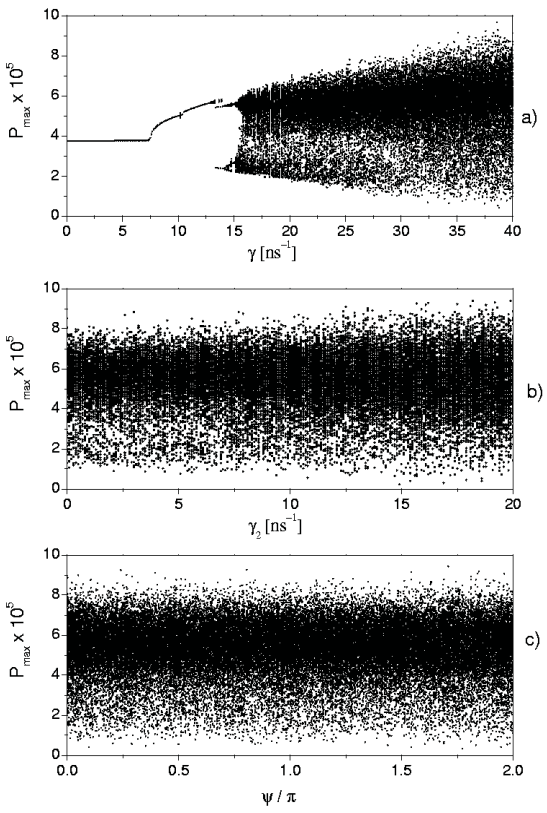

Fig. 14. Bifurcation diagram of the output power for(a) COF with the feedback strength γ as bifurcation parameter; (b) TDCF with γ_2 as bifurcation parameter; $\gamma_1 = 30\ \text{ns}^{-1}$, $\varphi = 0$ and $\psi = \pi/2$; (c) DCF with the MFB phase ψ as bifurcation parameter; $\gamma_1 = 30\ \text{ns}^{-1}$, $\gamma_2 = 10\ \text{ns}^{-1}$ and $\varphi = 0$. Each dot represents a peak of the output power [24].

3.3. Synchronization and message transmission

So far we have clarified different aspects of the transmitter laser dynamics under a TDCF. In what follows, we focus on the transmitter–receiver configuration and evaluate the synchronization properties. Since our final aim is to use the auxiliary branch to perform OOPSK encryption, it is important to characterize in advance the resynchronization time, i.e., the time required by the setup to synchronize when the link between master and slave lasers is interrupted. The inverse of the resynchronization time is an estimation of the maximum modulation rate that can be achieved with the OOPSK technique. We estimate the resynchronization time as the time needed by the system to achieve a correlation coefficient of 0.98 when starting from an initial uncoupled configuration, for which the correlation between emitter and receiver is close to zero [24]. Figure 15 shows the resynchronization time as a function of feedback strength for a laser under the influence of COF for different values of delay time τ and different coupling coefficient κ in a region where the system displays a chaotic behavior.

As shown in Fig. 15a, two regimes are observed for delay time $\tau = 0.5$ ns. For $\gamma > \kappa_r$ the resynchronization time grows linearly with a small slope and it is on the order of a few round-trip time. When γ becomes larger the resynchronization time grows exponentially. This last regime appears for $\gamma > 27\ \text{ns}^{-1}$ when $\kappa_r = 60\ \text{ns}^{-1}$ and for $\gamma > 33\ \text{ns}^{-1}$ when $\kappa_r = 90\ \text{ns}^{-1}$. The separation in the regimes comes from a competition between the coupling strength κ_r and the feedback strength γ. For $\kappa_r >> \gamma$ the first regime is dominant leading to a small resynchronization time; when both are similar, there is a transient competition, which induces large resynchronization time. Finally, no synchronization is observed for $\gamma >> \kappa_r$. Similar behavior is observed for a large delay time $\tau = 2$ ns (see Fig. 15b), although now the resynchronization time in the first regime grows linearly with a larger slope.

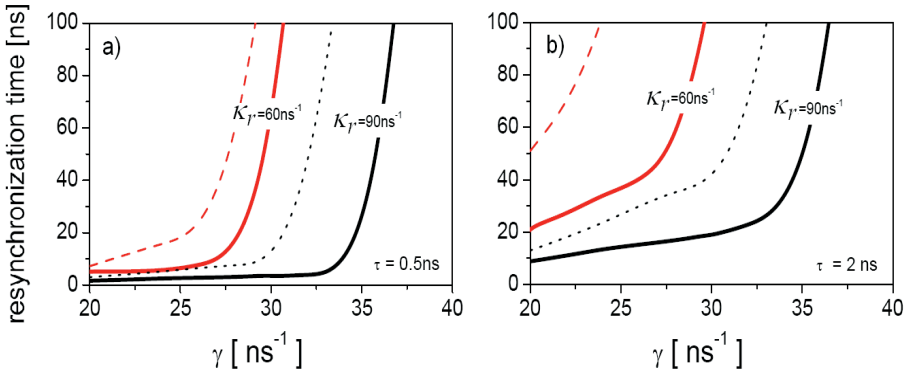

Fig. 15. Resynchronization time as a function of feedback strength for COF for $\varphi = 0$ and the delay time $\tau = 0.5$ ns (a) and $\tau = 2$ ns (b). Results are obtained from 100 random initial conditions. Thick lines show the average resynchronization time, while thin lines show the maximum value of those 100 realizations.

Figure 16a shows the calculated resynchronization time for a laser under the influence of a TDCF. The feedback strength of CFB is fixed to $\gamma_1 = 30\ \text{ns}^{-1}$, while that of MFB is varied. For zero MFB feedback strength the resynchronization time coincides with that of COF for $\gamma = 30\ \text{ns}^{-1}$. An increase in the MFB feedback strength up to $\gamma_2 = 20\ \text{ns}^{-1}$ leads only to a smooth increase in the resynchronization time up to a value of approximately 7 ns.

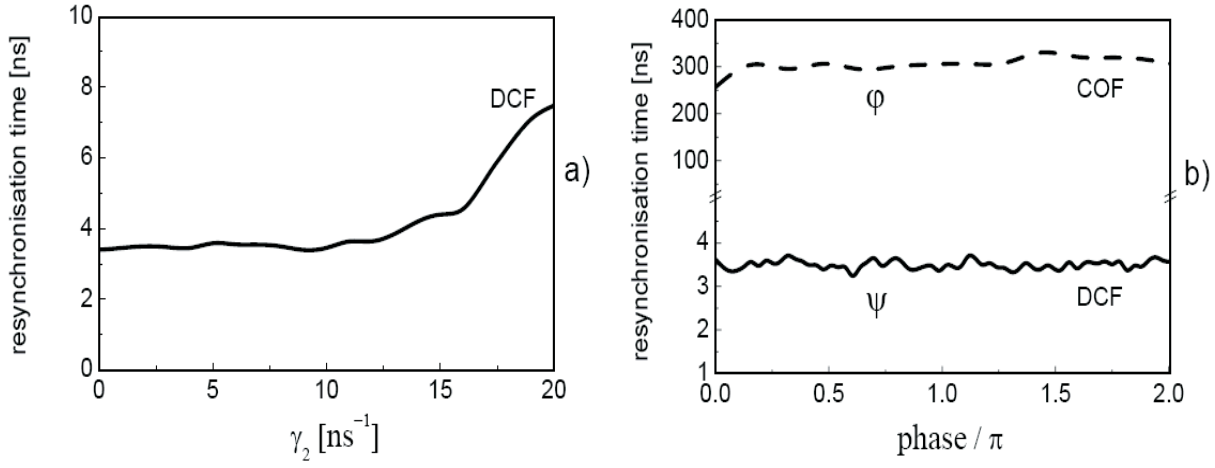

Fig. 16. Resynchronization recovery time as a function of different parameters (a) the feedback strength γ_2 of MFB for TDCF for $\gamma_1 = 30\ \text{ns}^{-1}$, $\varphi = 0$, $\psi = \pi/2$, (b) the feedback phase for the COF (dashed line) and for the TDCF (solid line). The parameters for the COF are $\gamma = 40\ \text{ns}^{-1}$ and $\tau = 0.5\ \text{ns}$. The parameters for the DCF are $\gamma_1 = 30\ \text{ns}^{-1}$, $\gamma_2 = 10\ \text{ns}^{-1}$, $\varphi = 0$, $\tau_1 = 0.5\ \text{ns}$, $\tau_2 = 0.3\ \text{ns}$, $\kappa_r = 90\ \text{ns}^{-1}$.

A first comparison of Figs. 15 and 16 shows that TDCF has some advantages over COF. When the feedback strength of COF is $40\ \text{ns}^{-1}$, the resynchronization time is approximately 300 ns, while for the DCF with $\gamma_1 = 30\ \text{ns}^{-1}$, $\gamma_2 = 10\ \text{ns}^{-1}$ the resynchronization time is approximately 3 ns (see Fig. 16a). In fact, we have found that, when using the DCF setup, we can reduce the resynchronization time by two orders of magnitude as compared with the COF setup. This decrease in the resynchronization time can be attributed to the fact that, for low feedback strength values, the MFB acts as a weak perturbation of the strong chaotic attractor generated by the CFB. This fact yields shorter resynchronization times as compared to the COF case. The solid line in Fig. 16b shows the resynchronization time as a function of MFB phase ψ for TDCF, for $\gamma_1 = 30\ \text{ns}^{-1}$, $\gamma_2 = 10\ \text{ns}^{-1}$, $\psi_m = \psi_S = 0$. The dashed line shows the resynchronization time as a function of optical feedback phase of the COF case for $\gamma = 40\ \text{ns}^{-1}$, $\varphi = 0$. It can be clearly seen from these results that the TDCF system resynchronizes much faster than the COF system for any value of the feedback phase. We have checked that these results also hold for any value of the COF phase ψ.

Now we consider the influence of a mismatch between the phases ψ of the slave laser with respect to that of the master laser on the cross correlation coefficient. Figure 17 shows the values of this coefficient in the plane $(\psi_s - \psi_m)$ for feedback strengths $\gamma_1 = 30\ \text{ns}^{-1}$, $\gamma_2 = 10\ \text{ns}^{-1}$ and the coupling coefficient $\kappa_r = 90\ \text{ns}^{-1}$.

Other parameters are identical for the master and slave lasers. It can be clearly seen that highest correlation coefficients are obtained when the two phases coincide, i.e., $\psi_m = \psi_s$, while the correlation degrades when the phases start to be different. Points *A* and *B* in Fig. 17 correspond to the operating points that will be considered later for message encoding and decoding using OOPSK encryption. The point *A* is chosen to have high correlation while the point *B* (or *B'*) corresponds to a state with low correlation.

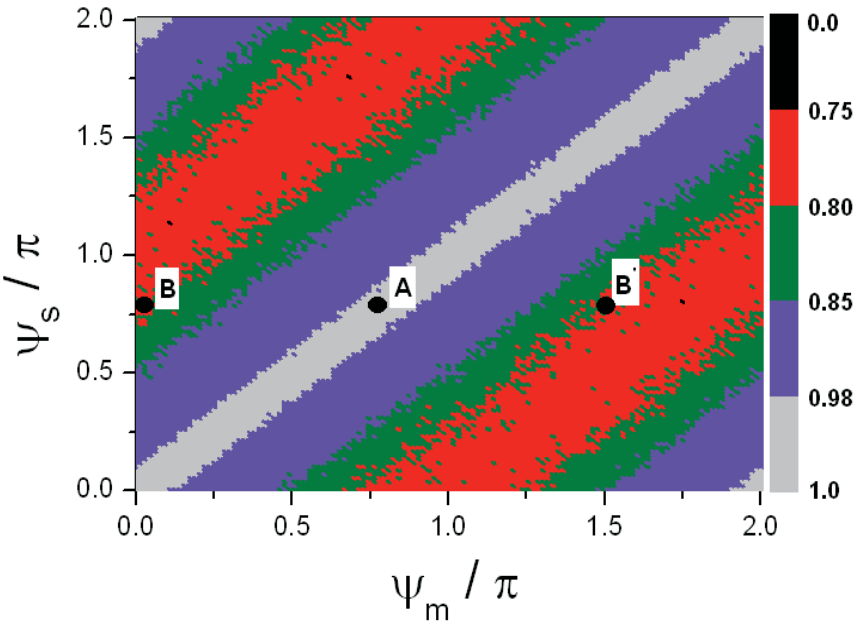

Fig. 17. Cross correlation coefficient in the ψ_m - ψ_s phase space. The other parameters are $\gamma_1 = 30\ \mathrm{ns}^{-1}$, $\gamma_2 = 10\ \mathrm{ns}^{-1}$, $\kappa_r = 90\ \mathrm{ns}^{-1}$, $\varphi_m = \varphi_S = 0$. A high degree of synchronization is characterized by light grey level. Phases are varied in 0.05 radian steps (taken from [26]).

3.4. Message transmission

An important issue in chaos based communication systems is the security of proposed setup. Schemes, such as chaos shift keying, chaos masking, and chaos modulation, require keeping the message amplitude small enough in order to avoid message recognition. In the OOPSK technique, the message is codified by changing the feedback phase of the master laser without introducing significant changes in the time trace or spectrum of the emitted light. In this setup, the slave laser for which the feedback phase is kept constant acts as a detector of the synchronization quality. When the feedback phases of the emitter and receiver coincide, the correlation between the outputs of the two systems is high, while it is low when the phases are different (as shown in Fig. 17). In our scheme, the phases φ of the COF branch is kept constant in both master and slave lasers while we study the phase shift keying method by varying the phase of the auxiliary branch. Figure 18 shows the pulse traces of the master laser operating in the chaotic regime at the point *A* (a) and at point *B* (b). It can be clearly seen that both time traces remain similar to each other. Figure 18c shows the power spectra of the time traces shown in Figs. 18a and 18b, while Fig. 18d shows the power spectra of the receiver system for the fixed phase $\psi_S = 0.75$ rad.

The power spectra of the emitter system for the operating points *A* and *B*, as shown in Fig. 18c, remain almost unchanged. On the contrary, the power spectrum of receiver laser changes, as shown in Fig. 18d, due to the coupling light that is uncorrelated with that generated by the receiver system. Figures 8e and 8f show the synchronization error defined as $\left|(P_m - P_s)/(P_m + P_s)\right|$ for different phases. For $\psi_m = \psi_s = 0.75$ rad (see Fig. 18e) the synchronization error is almost zero and the cross correlation coefficient approaches unity. On the other hand, for $\psi_m = 0$, $\psi_S = 0.75$ rad synchronization degrades, as shown in Fig. 18f, and the synchronization error is very high.

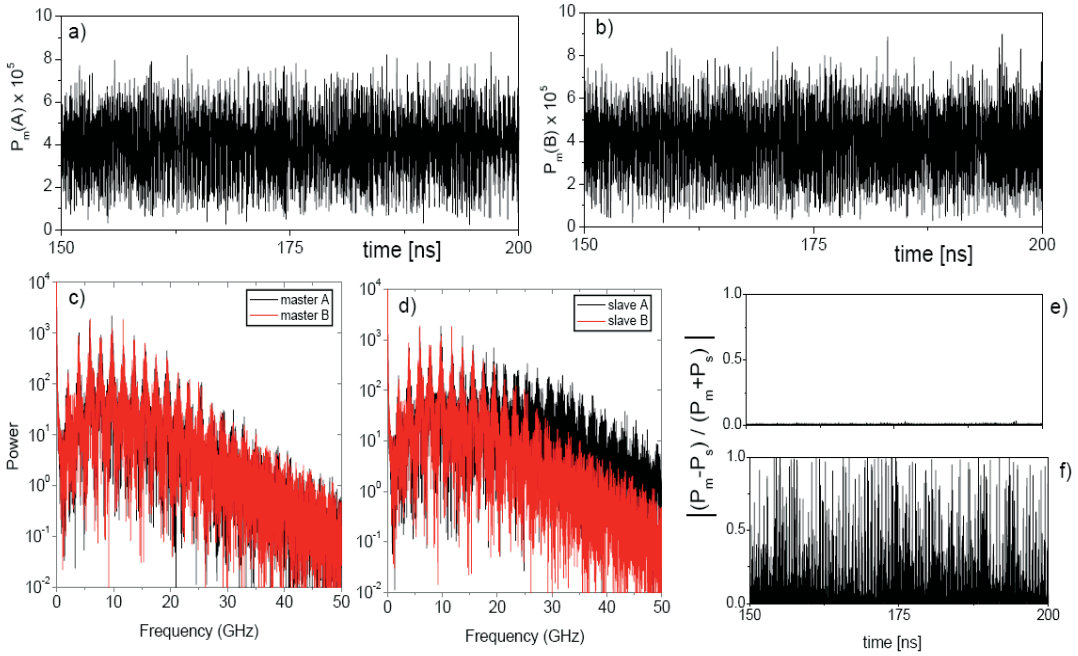

Fig. 18. (Color online) Calculated pulse traces of the emitter laser at point *A* (a) and point *B* (b) shown in Fig. 7. Power spectra of the master (c) and slave (d) lasers. Panels (e) and (f) show the synchronization error for $\psi_m = \psi_s = 0.75$ rad and $\psi_m = 0$, $\psi_S = 0.75$ rad, respectively. Parameters are the same as in Fig. 17.

Figure 19 depicts the process of 0.25-Gbit/s message OOPSK encryption. The top panel shows the digital message. Figure 19 (central panel) shows the synchronization error when the phase of the receiver laser is changed from 0.75 rad (bit "0") to 0 (bit "1"), i.e., from point *A* to point *B* in Fig. 17. Figure 19 (bottom panel) shows that the message can be successfully recovered after a standard filtering process. Thus, the proposed setup can distinctly increase the bit rate compared with that previously obtained in [21].

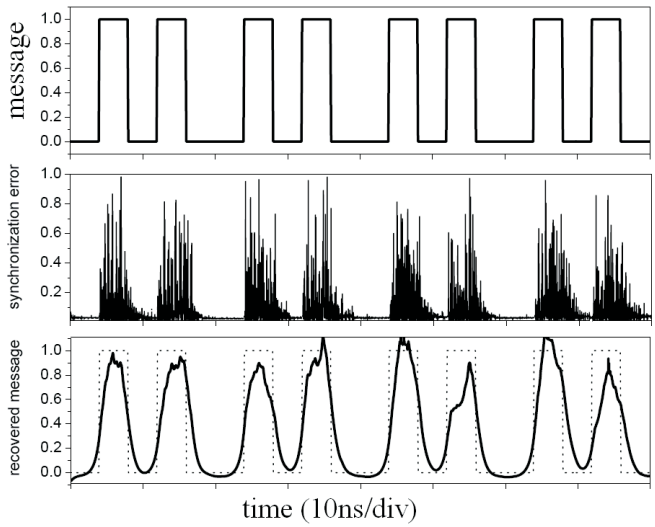

Fig. 19. On/off phase shift keying encoding and decoding of 0.25-Gb/s digital message. Top panel: encoded message. Central panel: decoded message represented by the synchronization error. Bottom panel: recovered message after filtering. The other parameters are the same as in Fig. 17 and [24].

4. Conclusions

In this review, we have studied the dynamics of an integrated device composed of a semiconductor laser and a longitudinal double cavity that provides delayed optical feedback. The double cavity feedback implies the existence of two feedback phases, which can play an important role in the dynamics. This extra degree of freedom leads to a more complex behavior, which in fact is already indicated when looking for the number and location of the fixed points. While in the more conventional case of using a single cavity, these steady states are located on the top of an ellipse in the $(N_S - \omega_S)$ plane, the ellipse in the double cavity case can be strongly distorted and can break into several bubbles. The number of coexisting steady states is also increased in the case of double cavity feedback, and chaotic behavior is found for lower values of the feedback strength. Furthermore, chaos appears already for quite short cavities, allowing for compact devices. We have shown that two of these devices can be synchronized when operating in the chaotic regime in a master-slave configuration. However, synchronization is degraded when there is a mismatch in the parameters of the master and slave system. Since the novelty of this scheme is the existence of two feedback phases, we have discussed the effect of a mismatch in these phases in detail. A mismatch in the air gap feedback phase turns out to have stronger effects in the master-slave cross-correlation than a mismatch in the material cavity feedback phase. However, for mismatches small enough, good quality synchronization is obtained. For the parameter values where good synchronization is achieved, it is possible to encode a message in the carrier using the chaos modulation technique. The message can be appropriately recovered at the receiver even for high bit rates. The codification method we employed is just an example of what can be done. While this codification technique is efficient and simple to implement, other codification methods could be used as well.

We have also studied the dynamics of a device composed of a semiconductor laser subject to a TDCF. The main advantages of this scheme over that of single cavity include the existence of two feedback strengths, two feedback phases, and two delay times that can be controlled separately. The results presented in this review show the following features: under appropriate conditions, this setup is capable of generating a robust chaotic waveform; two of these devices can be synchronized when operating in the chaotic regime in a master-slave configuration if some parameters are properly matched; a short resynchronization time, which is two orders of magnitude shorter than that of COF case, can be obtained with this scheme; and OOPSK encryption can be successfully applied at a rate of hundreds of Mbit/s. This means that such devices are promising candidates for fast on/off phase shift keying encryption.

We believe that our work provides a good basis for future study and, in particular, provides some pointers for more detailed investigations of multi-section integrated devices and their applications for chaos-based communication systems.

Acknowledgements

This study was supported by projects 307b/s of the Technical University of Moldova and Picasso IST-2005-34551. The author thanks C. Mirasso, P. Colet, and I. Fischer for useful discussions and expresses his gratitude for the hospitality in the group IFISC at the UIB, Palma de Majorca (Spain) and in the Laser Dynamics group at the WIAS, Berlin (Germany).

References

[1] A. Pikovsky, M. Rosenblum, and J. Kurths, Synchronization: A Universal Concept in Nonlinear Sciences, Cambridge University Press, Cambridge, England, 405 p., 2003.

[2] Apostolos Argyris, Dimitris Syvridis, Laurent Larger, Valerio Annovazzi-Lodi, Pere Colet, Ingo Fischer, Jordi García-Ojalvo, Claudio R. Mirasso, Luis Pesquera, and K. Alan Shore, Nature, 438, 343, (2005).
[3] C.R. Mirasso, P. Colet, and P. Garcia-Fernandez, IEEE Photon. Tech. Lett., 8, 299, (1996).
[4] V. Annovazzi-Lodi, S. Donati, and A. Scire, IEEE J. Quantum Electron., 32, 953, (1996).
[5] S. Sivaprakasam and K.A. Shore, Opt. Lett., 24, 466, (1999).
[6] I. Fischer, Y. Liu, and P. Davis, Phys. Rev. A, 62, 011801, (2000).
[7] A. Bogris, D.F. Kanakidis, A. Argyris, and D. Syvridis, IEEE J. Quant. Electron., 41, 469, (2005).
[8] S. Tang and J.M. Liu, Opt. Lett., 26, 596, (2001).
[9] N. Gastaud, S. Poinsot, L. Larger, J.M. Merolla, M. Hanna, J.P. Goedgebuer, and E. Malassenet, Elect. Lett., 40, 898, (2004).
[10] F.Y. Lin and M.C. Tsai, Opt. Express, 15, 302, (2007).
[11] B. Krauskopf and D. Lenstra (Eds.), Fundamental Issues of Nonlinear Laser Dynamics, AIP Conference Proceedings, 548, (2000).
[12] Toni Perez, Mindaugas Radziunas, Hans-Juergen Wuensche, Claudio R. Mirasso, and Fritz Henneberger, IEEE Photon. Technol. Lett., 18, 20, 2135, (2006).
[13] S. Bauer, O. Brox, J. Kreissl, B. Sartorius, M. Radziunas, J. Sieber, H.J. Wunsche, and F. Henneberger, Phys. Rev. E, 69, 016206, (2004).
[14] C. Simmendinger and O. Hess, Physics Lett. A, 216, 97, (1996).
[15] F.R. Ruiz-Oliveras and A.N. Pisarchik, Opt. Express, 14, 12859, (2006).
[16] Yun Liu and Junjii Ohtsubo, IEEE J. Quant. Electron., 33, 1163, (1997).
[17] F. Rogister, P. Mégret, O. Deparis, M. Blondel, and T. Erneux, Opt. Lett., 24, 1218, (1999).
[18] F. Rogister, D.W. Sukow, A. Gavrielides, P. Mégret, O. Deparis, and M. Blondel, Opt. Lett., 25, 808, (2000).
[19] V.Z. Tronciu, H.-J. Wünsche, M. Wolfrum, and M. Radziunas, Phys. Rev. E, 73, 046205, (2006).
[20] S. Schikora, P. Hoevel, H-J. Wuensche, E. Schoell, and F. Henneberger, Phys. Rev. Lett., 97, 213902, (2006).
[21] Tilmann Heil, Josep Mulet, Ingo Fischer, Claudio R. Mirasso, Michael Peil, Pere Colet, and Wolfgang Elsäßer, IEEE J. Quant. Electron., 38, 1162, (2002).
[22] C.R. Mirasso, Application of semiconductor lasers to secure communications, Fundamental Issue of Nonlinear Laser Dynamics, Ed. by B. Krauskopf and D. Lenstra, 112, (2000).
[23] V.Z. Tronciu, C.R. Mirasso, and P. Colet, J. Phys. B: Atom. Mol. & Opt. Phys., 41, 155401, (2008).
[24] V.Z. Tronciu, I. Ermakov, P. Colet, and C.R. Mirasso, Opt. Comm., 281, 4747, (2008).
[25] V. Raúl, T. Pérez, and C.R. Mirasso, IEEE J. Quant. Electron., 38, 1197, (2002).
[26] R. Lang and K. Kobayashi, IEEE J. Quant. Electron., QE-16, 347, (1980).
[27] C.R. Mirasso, J. Mulet, and C. Masoller, IEEE Photon. Tech. Lett., 14, 456, (2002).
[28] F. Rogister, D. Pieroux, M. Sciamanna, P. Megret, and M. Blondel, Opt. Comm., 207, 295, (2002).
[29] A. Sanchez-Diaz, C.R. Mirasso, P. Colet, and P. Garcia-Fernandez, IEEE J. Quant. Electron., 35, 292, (1999).
[30] M. Peil, T. Heil, I. Fischer, and W. Elsässer, Phys. Rev. Lett., 88, 1741011, (2002).
[31] V. Annovazzi-Lodi, M. Benedetti, S. Merlo, T. Perez, P. Colet, and C.R. Mirasso, Phot. Tech. Lett., 19, 76, (2007).
[32] E. Schöll, Nonlinear Spatio-Temporal Dynamics and Chaos in Semiconductors, Cambridge University Press, Cambridge, 424 p., 2001.